Bulletin of the Seismological Society of America, Vol. 103, No. 5, pp. 2739–2751, October 2013, doi: 10.1785/0120120174

A Homogeneous Earthquake Catalog for Western Turkey and Magnitude of Completeness Determination

by Konstantinos M. Leptokaropoulos, Vassilios G. Karakostas, Eleftheria E. Papadimitriou, Aggeliki K. Adamaki, Onur Tan, and Sedat İnan

Abstract A catalog for earthquakes that occurred in western Turkey during the period 1964–2010 is compiled for achieving homogeneity for magnitudes. Data are obtained from the International Seismological Center (ISC), where earthquake magnitudes are reported in different scales and come from a variety of sources. For establishing a common magnitude expression, namely an equivalent moment magnitude M_w^*, new relations correlating the different magnitude scales with each other are derived from converting as many as possible of the magnitudes reported in the ISC bulletins. After magnitude conversions, the completeness magnitude M_c is sought by modifying the goodness-of-fit method of Wiemer and Wyss (2000) to become more appropriate for datasets with smaller sample size and higher M_c thresholds. The study region is divided into four smaller regions on the basis of spatial data homogeneity, while different periods of similar seismic network performance are recognized and tested to seek spatiotemporal variation of M_c. The results derived in each case are compared with those yielded by the application of both the original goodness-of-fit and maximum curvature methods and are found to be quite similar, although there are still cases with a difference exceeding 0.3 magnitude units. The goodness-of-fit method is very sensitive in the selection of the desirable percentage of fitting a power law (90% or 95%), whereas the proposed modification makes it independent of this level selection, and performing better especially for datasets that include events before 1990, when higher completeness magnitudes are evident.

Online Material: Earthquake catalog with equivalent moment magnitude for western Turkey.

Introduction

Seismicity catalogs constitute a major product of seismological research, while simultaneously providing a beneficial tool for a wide range of seismic data analyses. For this reason, the focal parameters, origin time, and magnitude of the events must be determined as precisely as possible. However, most earthquake catalogs are nonhomogeneous because of a variety of factors that depend on both random and systematic errors introduced during the acquisition process and the database construction procedure. Random errors arise from human-made observations on seismic arrival times and potential temporal failure of part of the seismological network, whereas systematic errors are related with modeling uncertainties of calculated travel times connected with the assumed velocity model, modification of the applied software, and nonlinearity of earthquake location process (Pavlis, 1986; Habermann, 1987; Husen and Hardebeck, 2011). The state of seismic networks over time and the associated spatial and instrumental heterogeneity are additional factors of paramount importance, as they considerably affect the level of earthquake detection. All of these uncertainties and variations over space and time lead to inhomogeneous catalogs, which in turn lead to significant data contamination and misinterpretations of the results in many kinds of analyses, such as seismicity rate evaluation and hazard assessment.

These problems are more evident when the analysis needs to include data from periods with durations on the order of decades and in regions where the coverage from the seismic network is sparse. Our study site, western Turkey (Fig. 1), exhibited insufficient network coverage for a long time, although it comprises one of the most rapidly deforming regions worldwide, with intense seismic activity and frequent strong earthquake occurrence. The complex interaction among the Arabian, Eurasian, and African lithospheric plates has led to diverse faulting systems in the Aegean and surrounding regions. The North Anatolian fault (NAF), a long right-lateral strike-slip fault system extending from the

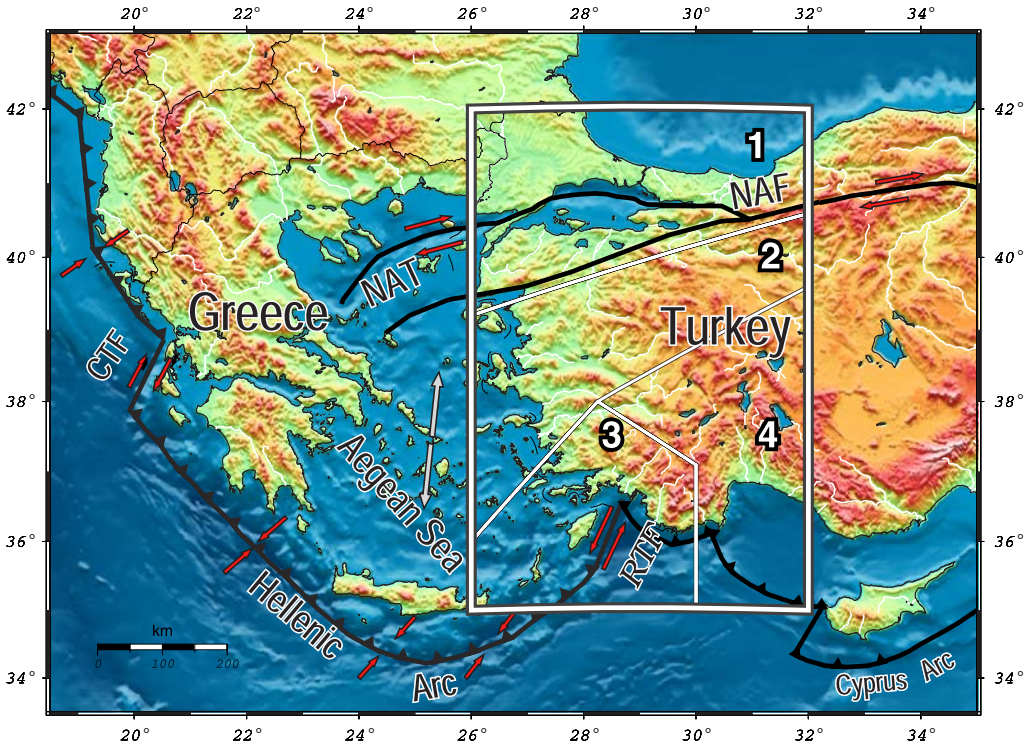

Figure 1. Morphological map of the Aegean Sea and surrounding areas with major active boundaries (black lines): the subduction zone (Hellenic arc) and the North Anatolian fault (NAF) with its westernmost extension, the North Aegean trough (NAT). The collision zone between the Apulian and Eurasian plates along with the Rhodes transform fault (RTF) and the Cephalonia transform fault (CTF) at the southeastern and western termination of the Hellenic arc, respectively, are also indicated along with the Cyprus arc at the southeast corner of the map. The white rectangle indicates the study site, and the thin white lines show the borders of the four areas. The color version of this figure is available only in the electronic edition.

eastern Turkey to the western Aegean Sea, is the one dominant geodynamic feature. Western Turkey also experiences an almost north–south-oriented continental extension due to the subduction and rollback of the eastern Mediterranean oceanic plate beneath the Aegean (Papazachos and Comninakis, 1969).

Historical and instrumental earthquake catalogs for Turkey and its surroundings have been available for decades (Pinar and Lahn, 1952; Ergin *et al.*, 1967, 1971; Soysal *et al.*, 1981; Güçlü *et al.*, 1986; Ambraseys and Finkel, 1995; Ambraseys and Jackson, 1998). Tan *et al.* (2008) compiled two digital databases for the regional seismicity in order to convert the available catalogs to a more accessible and manageable format. The first one includes parameters of the earthquakes that occurred between 2100 B.C. and 1963 A.D., and the second one comprises faulting parameters of the devastating earthquakes that occurred between 1938 and 2004. Inherent disadvantages in these earthquake catalogs of the instrumental period are mainly related to magnitude determination. To overcome this problem, empirical relations for converting a magnitude scale into moment magnitude were proposed for global (Ekström and Dziewonski, 1988; Scordilis, 2006; Bormann and Saul, 2008) or regional applications (Johnston, 1996; Papazachos *et al.*, 1997, 2002; Ambraseys, 2000; Baba *et al.*, 2000; Burton *et al.*, 2004; Ulusay *et al.*, 2004; Grünthal *et al.*, 2009; Yadav *et al.*, 2009; Akkar *et al.*, 2010; Deniz and Yücemen, 2010).

The motivation of this work is to achieve magnitude homogeneity in the earthquake catalog of western Turkey. For this purpose, all the reported magnitudes for each earthquake were collected, and then scaling laws among diverse magnitude scales were established, for magnitudes to be converted into an equivalent moment magnitude scale M_w^*, which is widely accepted as the most reliable one to express earthquake size. Magnitude estimates are available from the regional networks of Kandilli Observatory and Earthquake Research Center/Istanbul–Kandilli (ISK), Geodynamic Institute of the National Observatory of Athens (NOA), and Geophysics Department of the Aristotle University of Thessaloniki, along with magnitude estimates provided by International Seismological Center (ISC). We found out that ISC database includes all events that are partially included in the aforementioned regional catalogs; we therefore decided to use this source for our analysis.

After magnitude conversions and common expression for all events of our catalog, the completeness magnitude M_c and its possible variations, both in space and time, are sought. M_c determination is a crucial precondition that many kinds of seismicity—based methods require, and it indicates the minimum magnitude threshold, above which all the

events in a given catalog are recorded by the network over a specified time interval. In well-monitored regions, relatively low M_c can be achieved even for earlier periods (Hutton *et al.*, 2010). However, there are still many active tectonic areas where high quality catalogs with sufficient number of data cannot be obtained for periods on the order of decades because of the state and efficiency of the seismic network. Because knowledge on the state and evolution of the network is not available for our study site, we will seek its temporal efficiency by dividing the region into four smaller areas, enabling similarity in data quality and recording rates (Fig. 1), and then recognize periods of stable network performance. This analysis is preferred here instead of mapping M_c in a denser grid because of the data shortage in smaller areas. Nevertheless, we also attempted mapping M_c following some spatial constraints and then compared the completeness magnitudes resulting from each approach.

Data Processing

We used seismicity data from the ISC catalog, which provides revised information on earthquakes that took place up to 2010. We selected the events that were recorded in the study site since 1964, with a focal depth shallower than 60 km. Data from approximately 80 institutions are available for over 111,000 earthquakes that occurred during this period, with their magnitudes reaching 180,000 observations expressed in diverse magnitude scales. There are many events, nevertheless, with no magnitude assigned; and, therefore, they cannot be treated for the final catalog. The first step is to secure magnitude scale homogeneity by converting as many magnitudes as possible to a common magnitude scale, chosen here to be the equivalent moment magnitude M_w^*, taking as basis for this transformation the moment magnitude determined from the Global Centroid Moment Tensor (M_wGCMT). The technique applied for computing the parameters of the linear regressions between magnitude scales was the general orthogonal regression (see Appendix for details and formulation). Figure 2 shows all the resulted relations whereas the corresponding statistical information is provided in Table 1.

We preferentially sought for relationships between M_wGCMT and moment magnitudes provided by other institutions (Fig. 2a–c). First, moment magnitude from the National Earthquake Information Center (M_wNEIC) is considered identical with M_wGCMT (Scordilis, 2006) and therefore commonly taken as one data sample with the notation M_w. Next, moment magnitudes estimated by the Geodynamic Institute of the National Observatory of Athens (M_wNOA; Fig. 2a), the Mediterranean Network (M_wMED; Fig. 2b), and the Eidgenössische Technische Hochschule University of Zürich (M_wZUR; Fig. 2c) were selected and transformed; thus, 243 events with M_w^* were added in the catalog by this procedure. NOA is the only source that reports M_ws as low as 3.4, which enables extrapolation of the relationships to lower magnitudes and considerably increases the size of the final catalog. Given that moment magnitude is calculated with the same methodology (i.e., waveform inversion), we made the assumption that the relation between M_wGCMT and M_wNOA may be extrapolated for magnitudes lower than the range that the available data covers. Therefore, for each magnitude scale to be transformed, moment magnitude was taken either from GCMT or from M_w^*NOA (Fig. 2d–n, with different notation).

Surface-wave magnitudes, M_s, reported from ISC, NEIC, European Mediterranean Seismological Center (EMSC), and International Data Center (IDC) were then converted into M_w^* (Fig. 2d–g), along with body-wave magnitudes, m_b (Fig. 2h–k), reported from the same sources. Local magnitudes, M_L, from ISK and NOA (Fig. 2l–m), as well as duration magnitude, M_D, from NOA (Fig. 2n) were correlated with M_w and, more importantly, the large number of the M_D estimated from ISK. The problem with this latter magnitude lies at the lack of commonly existing M_D with M_w; therefore, M_DISK was correlated with the equivalent moment magnitude, as yielded from the conversion of body-wave magnitude from ISC (M_w^{bISC}; Fig. 2o). The advantages of this conversion are the large number of observations (pairs of magnitudes for the same events) and the wide magnitude range covered. In this way, we managed to treat events with magnitude as low as M_DISK 3.5. Figure 2o illustrates that linear regression cannot adequately simulate this relation, and a second degree polynomial fitting therefore is preferred.

Magnitude conversion into M_w^* is accomplished by giving priority to certain magnitude scales and estimates and then following a rule for adopting the final M_w^*. When M_wGCMT or equivalently M_wNEIC were available, these were directly adopted as M_w^* in our catalog. If M_w was estimated from a different source, then the higher conversion priority was set in which the root mean square (rms) error was lower; thus, M_w^*MED, was first preferred, then M_w^*ZUR, and finally M_w^*NOA. For the earthquakes with reported magnitudes in other magnitude scales, the conversion was performed for all the assigned magnitudes (except M_DISK), and the final M_w^* was estimated as a weighted average of all the available magnitudes, with a normalized weight inversely proportional to their rms errors. Finally, if the only available magnitude was M_DISK, then it was estimated from the second-degree polynomial. Thus an integrated catalog is achieved that is revised so as to be homogeneous in the magnitude scale and comprising 9875 events, with M_w^* ranging from 3.5 to 7.6, extending from 1964 to 2010, and from 35.00° N to 42.00° N latitude and 26.00° E–32.00° E longitude (Fig. 3). Ⓔ This catalog is available in the electronic supplement to this article.

Identification of Completeness Magnitude

The evaluation of M_c is usually accomplished by following two major approaches, the network-based (Schorlemmer and Woessner, 2008; Mignan *et al.*, 2011) and the catalog-based methods. There are two groups of catalog-based methods. The first one relies on the fact that the detection threshold due to the noise decreases during the night, and therefore

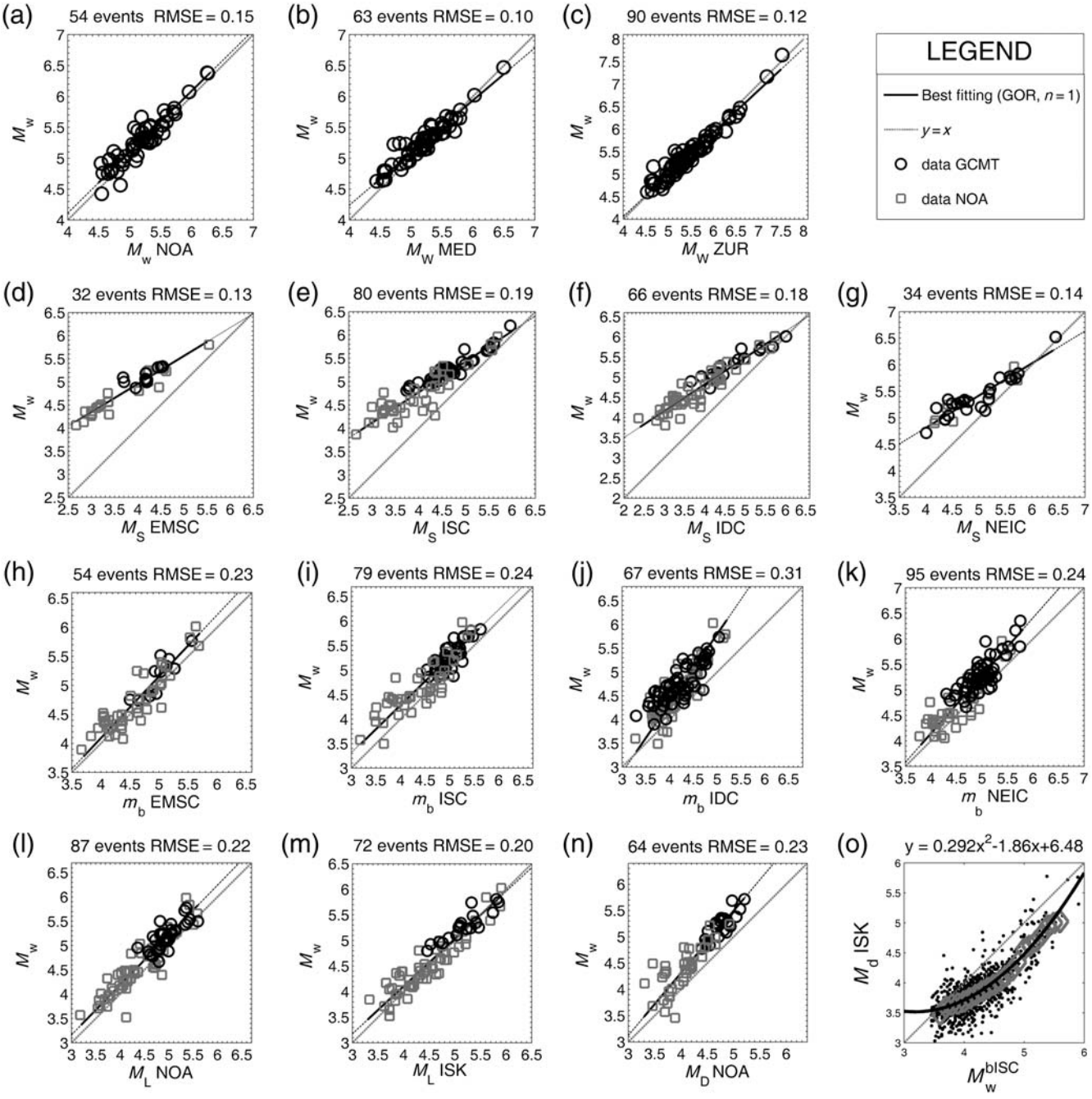

Figure 2. Magnitude relations between various scales and institutions and M_wGCMT (black circles) or M_w^*NOA (gray squares). The solid lines indicate the general orthogonal regression linear fitting, whereas the dashed lines indicate the bisector. For a better representation, data were plotting after the addition of three random decimal digits to the x and y values. The number of pairs and the root mean square error (RMSE) are shown above each frame. Figure 2o shows the second-degree polynomial fitting of M_DISK to the equivalent moment magnitude as it was calculated from the conversion of body-wave magnitude reported from ISC (M_w^{bISC}). The diamonds correspond to the average values of M_DISK per M_w^{bISC} unit.

M_c is determined by considering the day-to-night ratio of earthquake frequency (Rydelek and Sacks, 1989; Taylor *et al.*, 1990). The second group contains methods that follow the assumption of self-similarity of earthquake production, such that the frequency–magnitude distribution of earthquakes can be simulated by a power law, that is, the Gutenberg–Richter (G-R) law. The most frequently applied methods of this group are the entire magnitude range method (Ogata and Katsura, 1993; modified by Woessner and Wiemmer, 2005), the maximum curvature (MAXC) method (Wiemer and Wyss, 2000), the goodness-of-fit test (GFT) (Wiemer and Wyss, 2000), the M_c determination by b-value instability (Cao and Gao, 2002), and the median-based analysis of the segment slope (Amorèse, 2007). In an effort

Table 1
Empirical Relations for Magnitude Scales Transformation

Relation	Source	b	a	rms error	R^2	Number of Events Used and Their Magnitude Range
$M_w^* = a + bM_w$	NOA	0.99 ± 0.006	0.17 ± 0.162	0.15	0.93	54 (4.5–6.3)
	MED	0.85 ± 0.003	0.84 ± 0.074	0.10	0.95	90 (4.4–6.5)
	ZUR	0.93 ± 0.001	0.33 ± 0.037	0.12	0.97	63 (4.5–6.5)
$M_w^* = a + bM_s$	EMSC	0.61 ± 0.003	2.52 ± 0.042	0.13	0.95	32 (2.6–4.6)
	ISC	0.65 ± 0.002	2.15 ± 0.033	0.19	0.93	80 (2.8–6.0)
	IDC	0.66 ± 0.002	2.18 ± 0.027	0.18	0.94	66 (2.4–6.0)
	NEIC	0.61 ± 0.004	2.38 ± 0.010	0.14	0.92	34 (4.0–5.9)
$M_w^* = a + bm_b$	EMSC	1.06 ± 0.010	-0.15 ± 0.219	0.23	0.90	54 (3.7–5.6)
	ISC	0.98 ± 0.006	0.38 ± 0.128	0.24	0.90	79 (3.2–5.6)
	IDC	1.46 ± 0.021	-1.49 ± 0.385	0.31	0.87	67 (3.5–5.0)
	NEIC	1.13 ± 0.007	-0.39 ± 0.169	0.24	0.89	95 (3.9–5.7)
$M_w^* = a + bM_L$	NOA	1.03 ± 0.004	0.08 ± 0.090	0.23	0.90	54 (3.5–5.5)
	ISK	0.93 ± 0.003	0.39 ± 0.070	0.20	0.94	72 (3.6–6.0)
$M_w^* = a + bM_D$	NOA	1.18 ± 0.010	-0.43 ± 0.182	0.23	0.91	64 (3.4–5.2)

The conversion form is shown in the first column. The second column gives the data source. The a and b values of the general orthogonal regression fitting, along with their standard errors are shown in the third and fourth column, respectively. The next three columns provide information on the rms error, linear correlation coefficient (R^2), number of observations, and the respective magnitude range.

to determine M_c, Woessner and Wiemer (2005) and Mignan and Woessner (2012) reviewed and applied these methods and then compared their performance and stability.

The method applied here is based upon the GFT, proposed by Wiemer and Wyss (2000). The procedure they followed is that a power law, as a function of minimum magnitude, M_i, is fitted for events with $M \geq M_i$ by application of maximum-likelihood estimation. The synthetic data, that is, the distribution of magnitudes that represent a perfect fit to the power law, is constructed in this way. Then the normalized, absolute difference (R) between the cumulative number of observed events (N_o) and the simulated ones (N_s) in each magnitude bin is computed and mapped according to the formula

$$R = \frac{\sum_{M_i}^{M_{max}} |N_o - N_s|}{\sum_i N_o}. \quad (1)$$

If the dataset above a specific magnitude M_i is incomplete, R will be high. A model is found at an R-value at which a predefined percentage (usually 90% or 95%) of the observed data is modeled by a straight line, which means that 90% or 95% of the observed data can be simulated by the specific power law (Woessner and Wiemer, 2005).

A modified approach of this method is introduced and applied here, the modified goodness-of-fit test (MGFT). A synthetic dataset of N_i events is created by distributing random numbers according to the respective G-R law (Zechar, 2010), for which N_i is the cumulative number of events with $M \geq M_i$ in the observed dataset. After k iterations of this process, k synthetic catalogs are created. Here, we are interested only in frequency–magnitude distributions (FMD) of the events and not in their spatial and temporal parameters (epicenter location, origin time). Therefore, the synthetic catalogs consist of events for which the only free parameter is the magnitude. We chose k to be equal to 1000 and, instead of comparing the offset between real values and theoretical distribution, 1000 synthetic catalogs comprising random events with the same data number and magnitude distribution are constructed for each magnitude bin. Thus, one more parameter (the occurrence frequency in each magnitude bin) is introduced. Starting from a minimum magnitude M_i, parameters a and b of the G-R law are calculated following a maximum-likelihood estimation for all events, with $M_i \leq M \leq M_{max}$. According to Aki (1965), the b-value estimator is as follows:

$$b = \frac{1}{\ln(10)[\langle M \rangle - (M_c - \Delta M/2)]}, \quad (2)$$

in which $\langle M \rangle$ is the sample mean of the events considered and ΔM is the binning width of the catalog, equal to 0.1 in the present study. The same author also estimated the b-value accuracy (σ_b) as

$$\sigma_b = \frac{b}{\sqrt{N}}, \quad (3)$$

in which N stands for the sample size. The difference between each one of these synthetic datasets and the observed ones is calculated following equation (1), and an average value of these differences is derived. Then, the whole procedure is repeated by considering M_{i+1} as minimum magnitude. A new G-R law is retrieved (by estimating the new a and b values and given N_{i+1} as the cumulative number of observed events), with $M \geq M_{i+1}$. The mean values of the differences between the real FMD and the one derived from the synthetic catalogs for each magnitude bin are computed and mapped. The residuals are rather higher in this case, but there is an obvious minimum point; therefore, instead of considering an arbitrary selected level of fitting a power law, a more objective criterion is being applied.

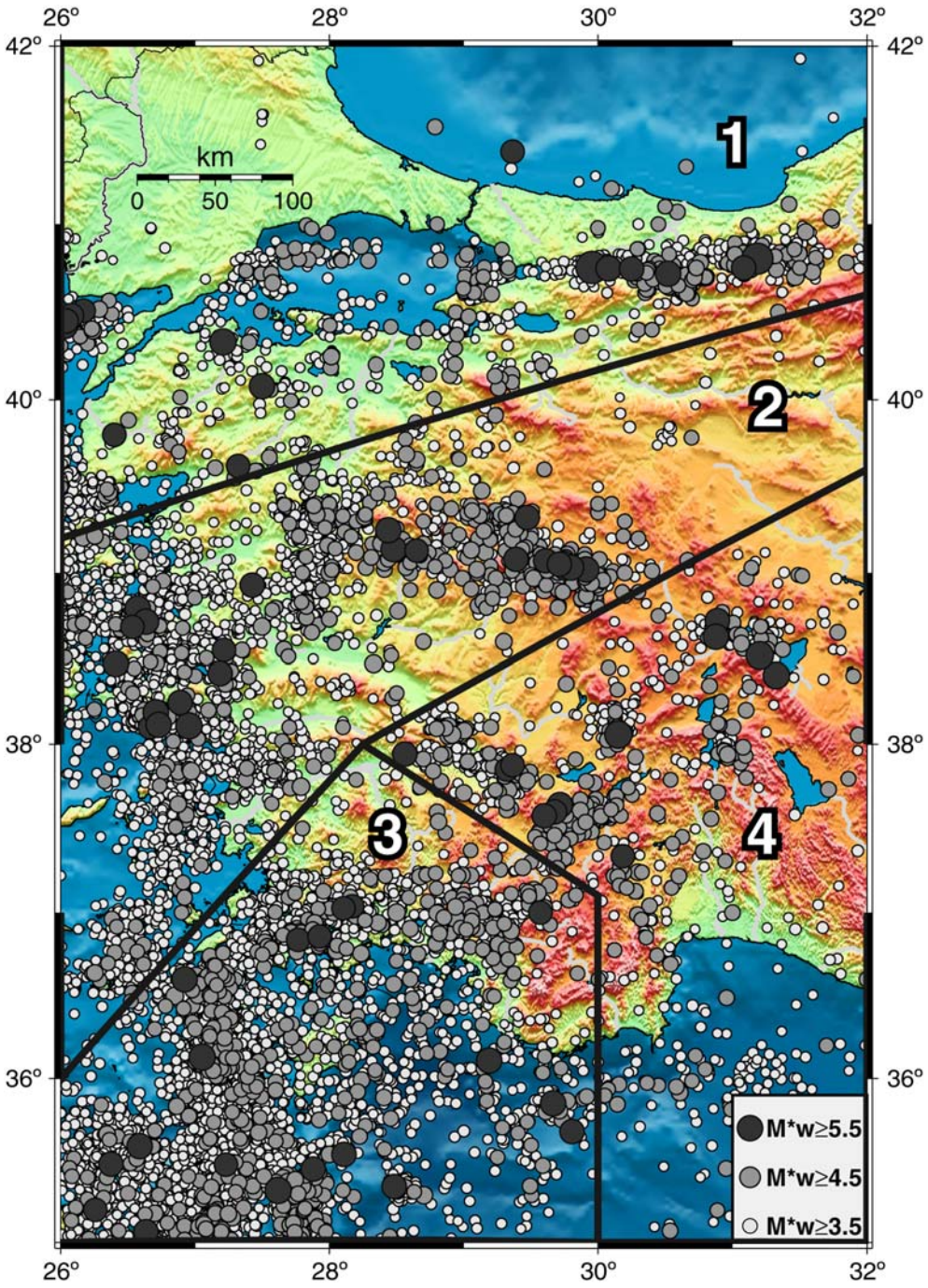

Figure 3. Spatial distribution of earthquakes epicenters during 1964–2010 in the study site (areas 1–4 are also here depicted) after the catalog compilation, with magnitudes expressed as M_w^*. The color version of this figure is available only in the electronic edition.

M_c Results and Discussion

The compiled catalog so far is considered homogeneous concerning the magnitude determination and is now elaborated for completeness magnitude, M_c, identification. The first step is to search for periods characterized by a relatively stable recording rate of earthquakes. Figure 4 shows the cumulative number of events, smoothed over three-year periods and above M_i in linear scale for each one of the four study areas. The periods were selected on the basis of a relatively stable number of recorded events for each dataset, and they are indicated by numbers and separated with dashed lines in Figure 4. It is evident that after the early 1990s the seismic network has become more efficient as the detection level of smaller earthquakes gradually increases. We then investigated M_c during the aforementioned periods. Moreover, some additional time windows were also tested in order to validate the robustness of the retrieved results and their temporal variation.

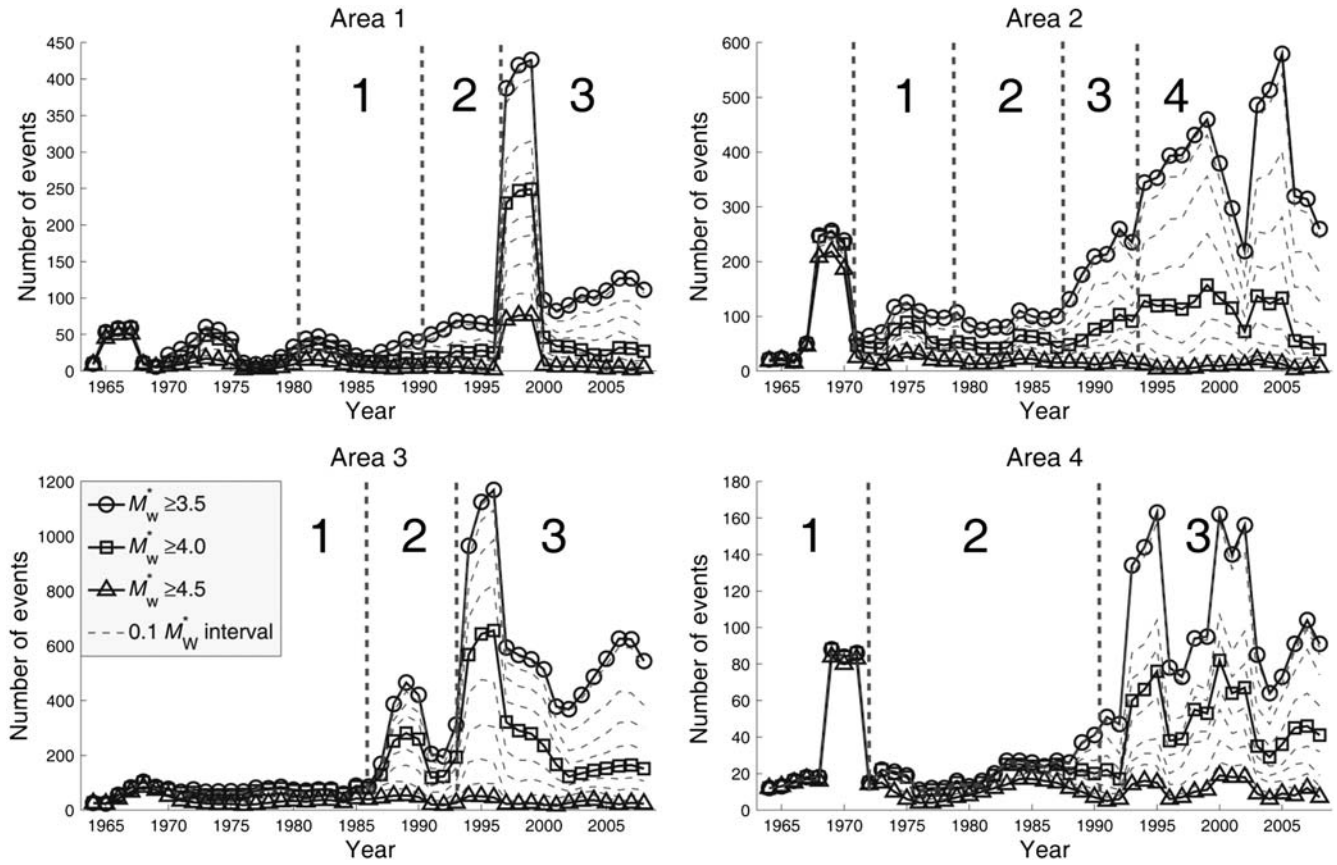

Figure 4. Cumulative number of events per magnitude bin (dashed lines, 0.1 magnitude-unit step; solid lines, 0.5 magnitude-unit step) per three-year periods in linear scale. Each year in the x axis indicates the starting time of a three-year period.

Table 2

M_c Results Yielded for Each Area and Period by the Application of Different Methods

Area	Period	MAXC	GFT(90%)	GFT(95%)	MGFT	$b_{(MGFT)}$
1	1981–1990	4.4	4.0	4.7	4.3	1.16 ± 0.162
	1991–1998	3.7	3.6	3.7	3.7	1.18 ± 0.101
	1999–2010	3.7	3.6	3.7	3.7	0.99 ± 0.039
	1999	3.7	4.1	–	4.2	1.06 ± 0.083
	2000–2010	3.6	3.6	–	3.7	1.32 ± 0.075
2	1971–1978	4.0	4.2	–	4.4	1.12 ± 0.125
	1979–1988	3.8	3.7	–	3.8	1.01 ± 0.062
	1989–1995	3.7	3.7	3.7	3.7	1.30 ± 0.061
	1996–2010	3.7	3.7	–	3.8	1.82 ± 0.053
	1996–2004	3.8	3.8	–	3.9	2.06 ± 0.088
	2005–2010	3.6	3.6	–	3.7	1.69 ± 0.070
3	1968–1986	4.5	4.4	4.7	4.7	1.44 ± 0.122
	1987–1994	4.2	3.9	4.1	4.2	1.40 ± 0.071
	1995–2010	3.8	3.9	4.5	3.8	1.69 ± 0.044
	1987–2010	3.9	3.9	4.4	3.9	1.69 ± 0.043
4	1971	4.7	4.6	4.7	4.7	1.51 ± 0.203
	1972–1990	4.5	4.5	4.8	4.5	1.52 ± 0.183
	1991–2010	3.7	3.7	3.7	3.7	1.09 ± 0.044
	1982–1993	4.1	4.7	–	4.5	1.31 ± 0.194

Maximum curvature method (second column), 90% and 95% goodness-of-fit test (third and fourth columns, respectively) and modified goodness-of-fit test (fifth column). The b-value that yielded from the final assumption and its standard error is shown in the last column. Cells below the dashed lines provide information for additional testing periods.

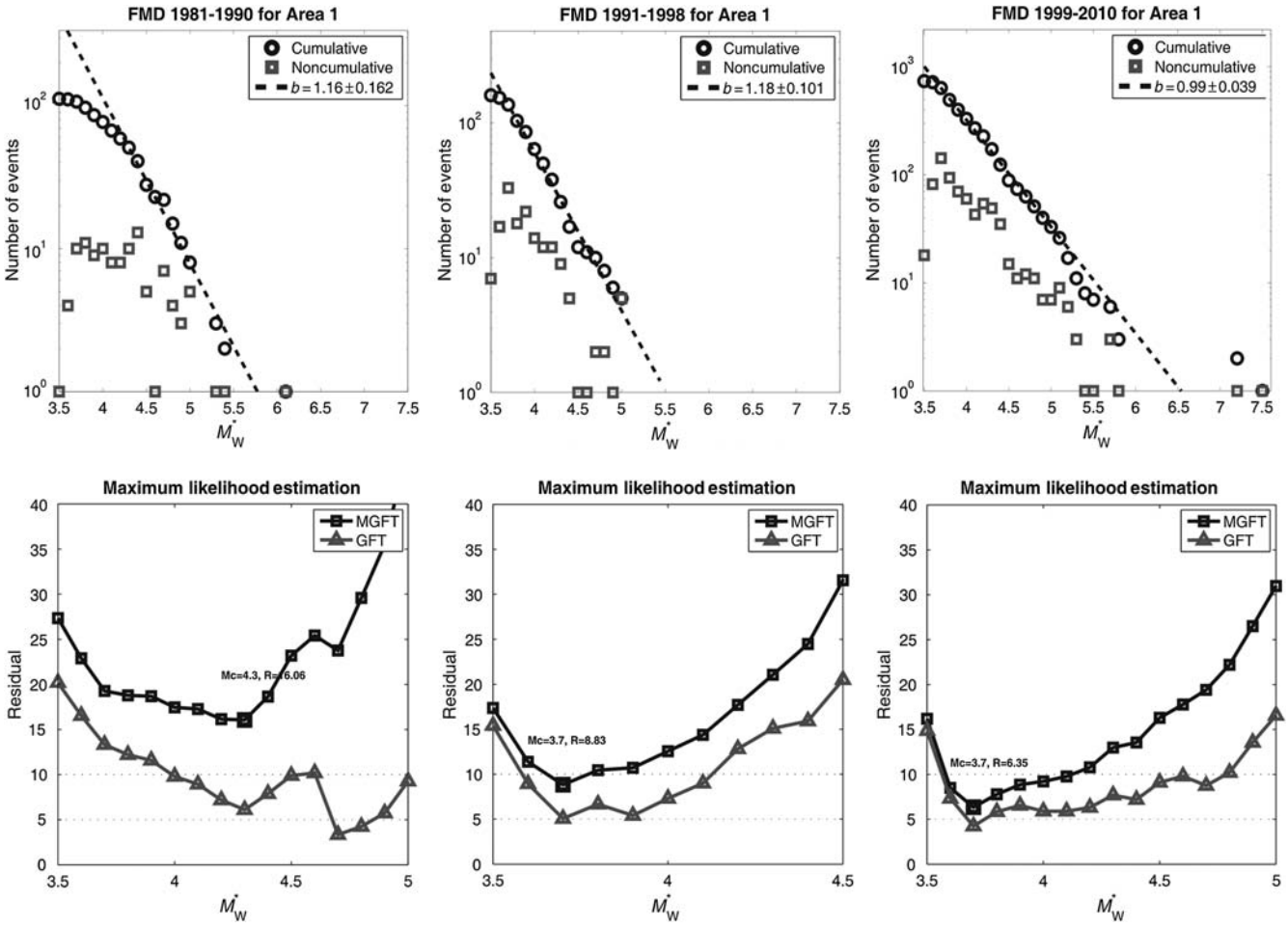

Figure 5. FMD (upper frames) for area 1 during the three selected periods. Noncumulative (squares) and cumulative (circles) number of events per magnitude bin are shown, along with the best fitting curve as derived from the MGFT (lower frame) for the respective time intervals. The gray line indicates the difference between the observed data and the theoretical distribution (power law), yielding from the maximum-likelihood estimation as a function of magnitude (GFT). The black line indicates the average difference between the observed data and the 1000 synthetic catalogs of random events following the MGFT power law. The lower and upper dashed lines indicate the 5% and 10% residuals, respectively.

Comparison of the results derived by application of the proposed technique with the ones derived from MAXC and GFT methods is summarized in Table 2.

For area 1 (Fig. 5), all approaches yielded the same M_c after 1991, with the GFT(90%) underestimating the M_c by 0.1 unit. For the first period, when data are more sparse, a 0.7 magnitude range appears between the results of GFT (90%) and GFT(95%), while MAXC and MGFT imply an intermediate M_c value. For area 2 (Fig. 6), the 95% fitting a power law could not be achieved in three out of the four cases. The other three methods demonstrate identical results after 1979, with maximum difference of 0.1 unit and the MGFT method providing more conservative results. For the earlier period, M_c is equal to 4.0 according to MAXC, and it is 0.2 and 0.4 units higher when GFT(90%) and MGFT, respectively, are applied. Quite different results were obtained for area 3 (Fig. 7), where, for the first period (1968–1986), the GFT(95%) and MGFT methods demonstrate the most conservative values of M_c, 0.2–0.3 magnitude units higher than the other two methods suggest. For the second period (1987–1994) the higher M_c values are calculated by MAXC and MGFT, and they are 0.1–0.3 units higher than the others. For the last period (1995–2010), the completeness magnitude is equal to 3.8–3.9, but the GFT(95%) suggests a significantly higher value of 4.5, which is also much higher than the ones calculated for the previous period. Finally, the MAXC and MGFT methods are in total agreement in area 4 (Fig. 8). The original GFT methods also provide similar results in general, but GFT(95%) indicates the unrealistic value of 4.8 as the M_c for the second period.

Investigations of the M_c spatial distribution were attempted on the nodes of a normal grid superimposed onto the study site. The available data were roughly sufficient for such analysis (Fig. 9). Evaluation was performed after 1995 in order to secure a relatively stable coverage from the seismic network and avoid merging datasets with significant different statistical properties. M_c was sought in the cells of a $0.1° \times 0.1°$ grid, and the goodness of fit in cascade circular

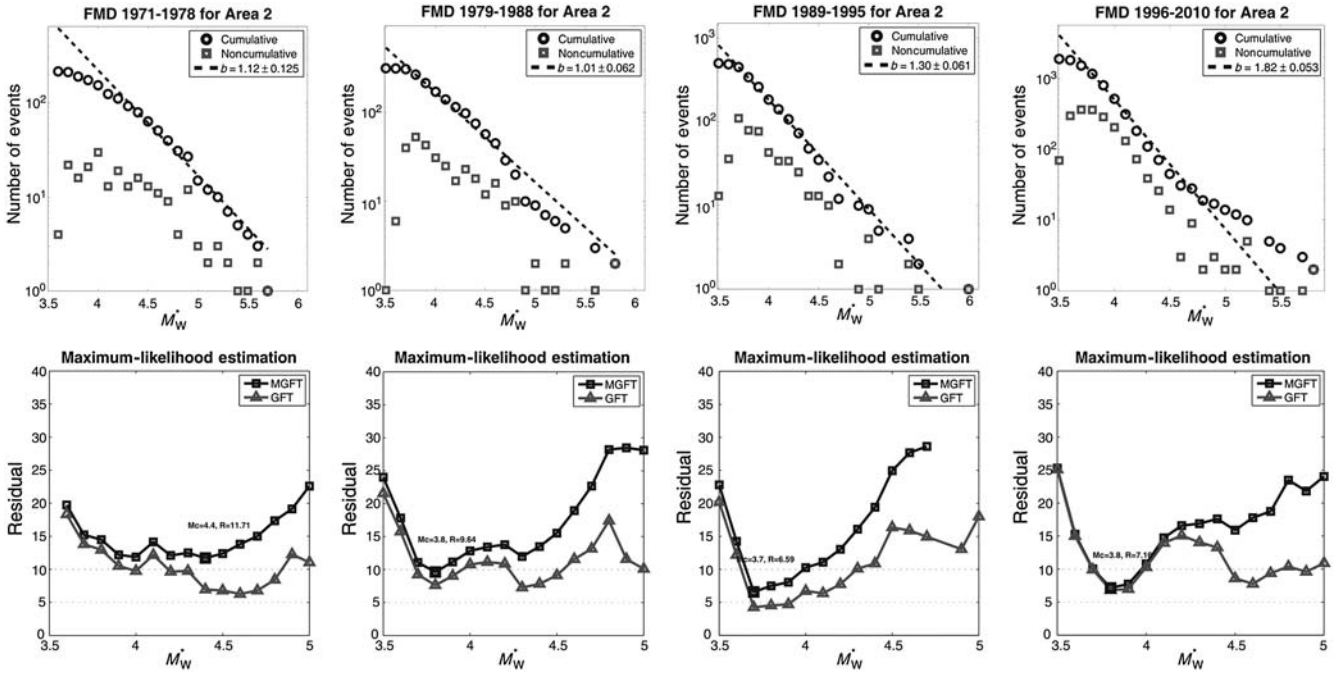

Figure 6. FMD (upper frames) and GFT (lower frame) for area 2 during the four selected periods. Description as in Figure 5.

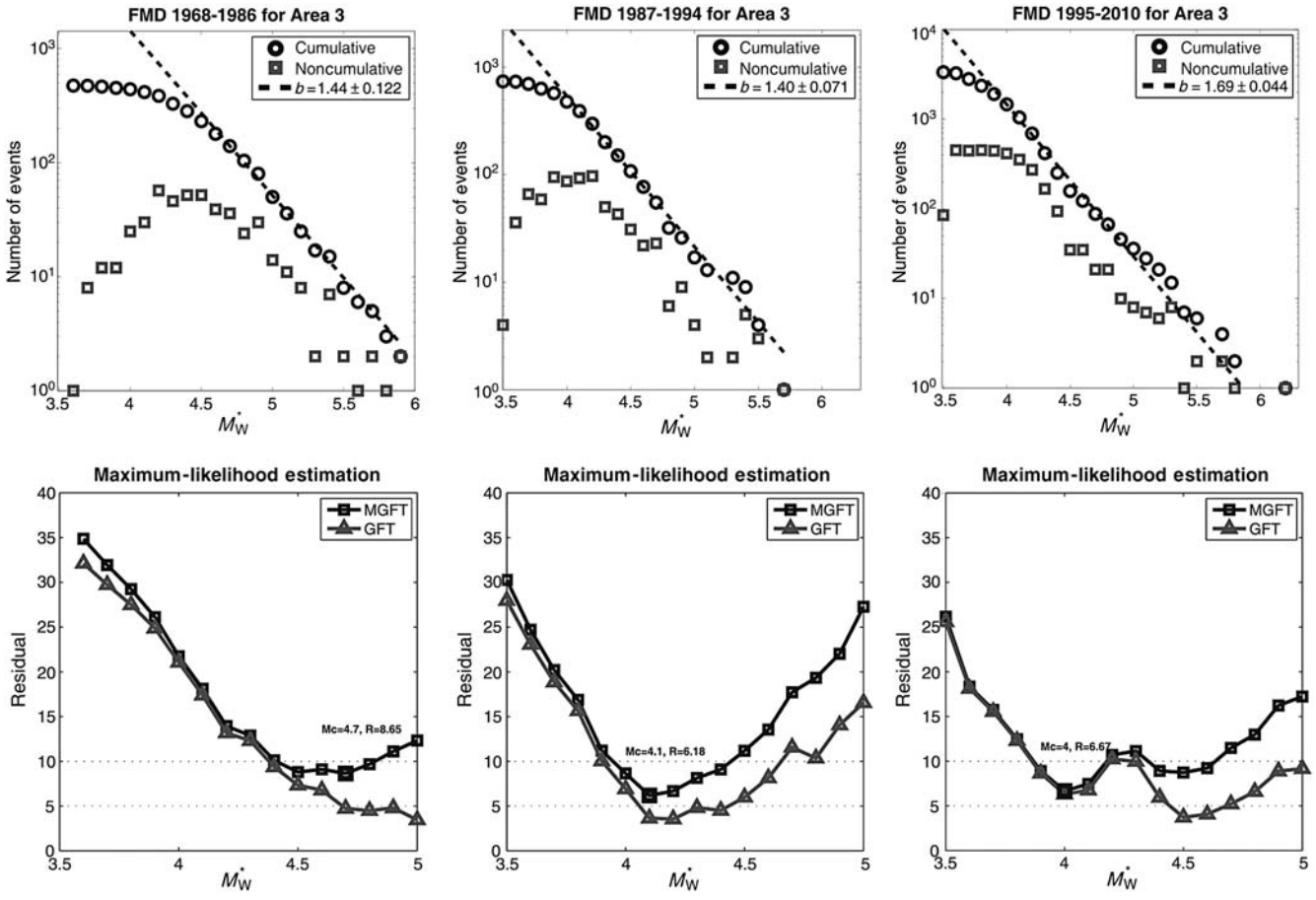

Figure 7. FMD (upper frames) and GFT (lower frame) for area 3 during the three selected periods. Description as in Figure 5.

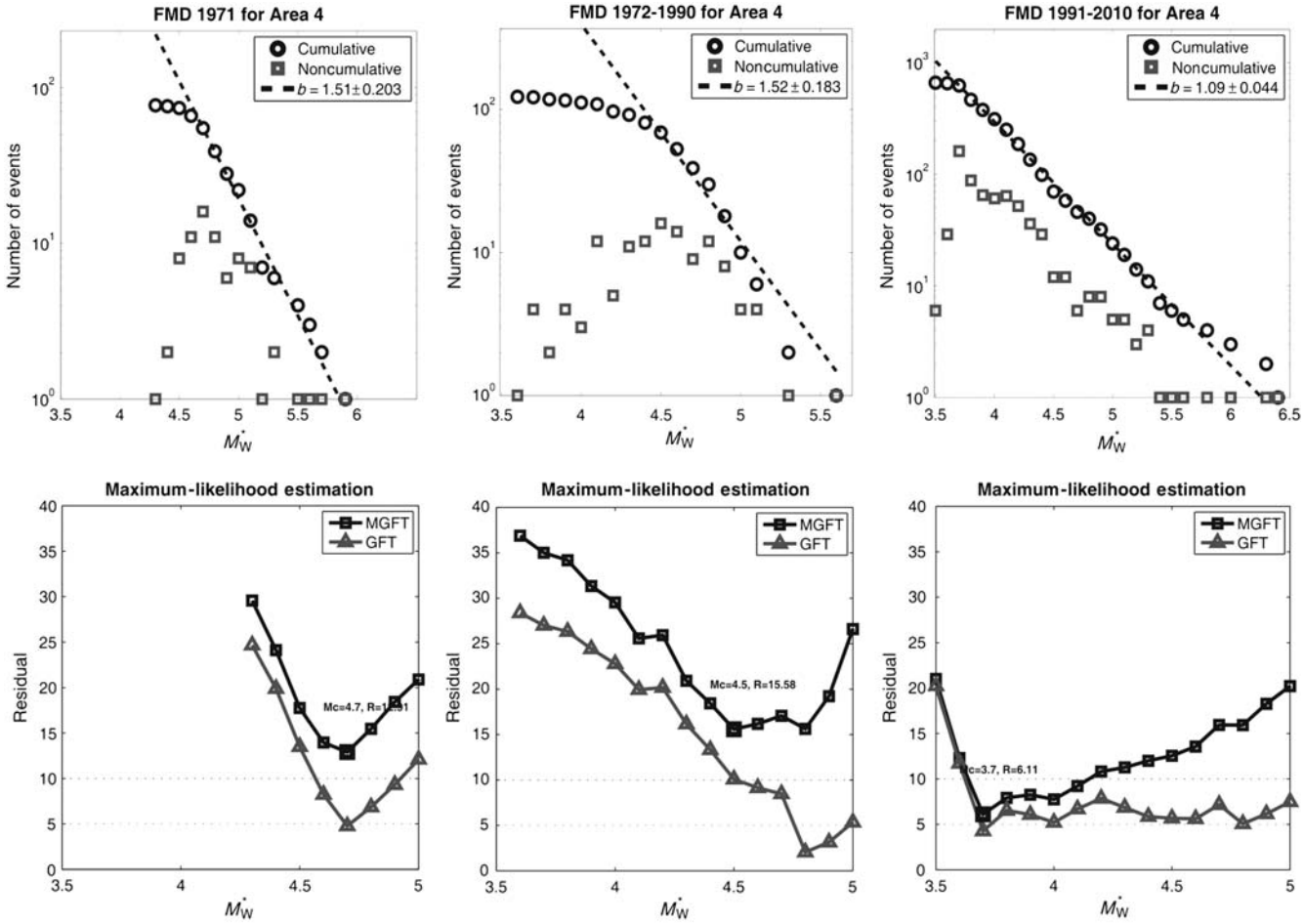

Figure 8. FMD (upper frames) and GFT (lower frame) for area 4 during the three selected periods. Description as in Figure 5.

areas with 40 km radii was employed for this scope. By constraining each circle to accommodate at least 50 events, and the magnitude range to least 1.5 magnitude units, the number of cells fulfilling these criteria corresponds to approximately 40% of the study site. The lower values of M_c were found mainly in the western and southwestern coastal areas and in the western segments of the NAF. These regions exhibit adequate network coverage and constant high rates of earthquake production, and thus a sufficient data sample is continuously available, even for shorter time intervals. Higher M_c thresholds are evident in the southeastern Aegean and along the eastern segments of the NAF. Nevertheless, the size of the available catalog indicates that it is more robust to seek M_c in broader areas rather than mapping it on the nodes of a dense grid where data sufficiency for such analysis is questionable.

Summary and Conclusions

This study aimed to achieve two distinctive goals, both of them of major importance for seismicity study in the complex and actively deforming region of western Turkey. First, an earthquake catalog that is homogeneous for the magnitude scale was compiled. After exhaustively exploring the different magnitudes available and seeking relations among them, scaling laws were derived for magnitude conversion from different scales into a common scale, that is, the equivalent moment magnitude, M_w^*. All reported magnitude scales from various institutions were engaged for this process to secure the inclusion of the maximum possible earthquake number in the final catalog. This catalog can then be considered as a reliable data source for the study site, with an adequate and homogeneous sample appropriate in diverse seismicity and seismic-hazard assessment studies.

The spatiotemporal properties of the catalog were sought after dividing the study site into four areas (Fig. 1) discriminated on the base of seismicity level. Then the detectability improvement of the regional seismic network through time was examined in an attempt to determine time intervals characterized by relatively constant seismicity rates recorded above predefined magnitude thresholds. The number and duration of the periods differ among the study areas.

The second goal of the present study was to evaluate the completeness magnitude, M_c, for each area and for specified periods (Table 2), to distinguish potential temporal fluctuations of M_c. To accomplish this aim, we modified the goodness-of-fit test of Wiemer and Wyss (2000) in order to be more effective for datasets composed of smaller sample

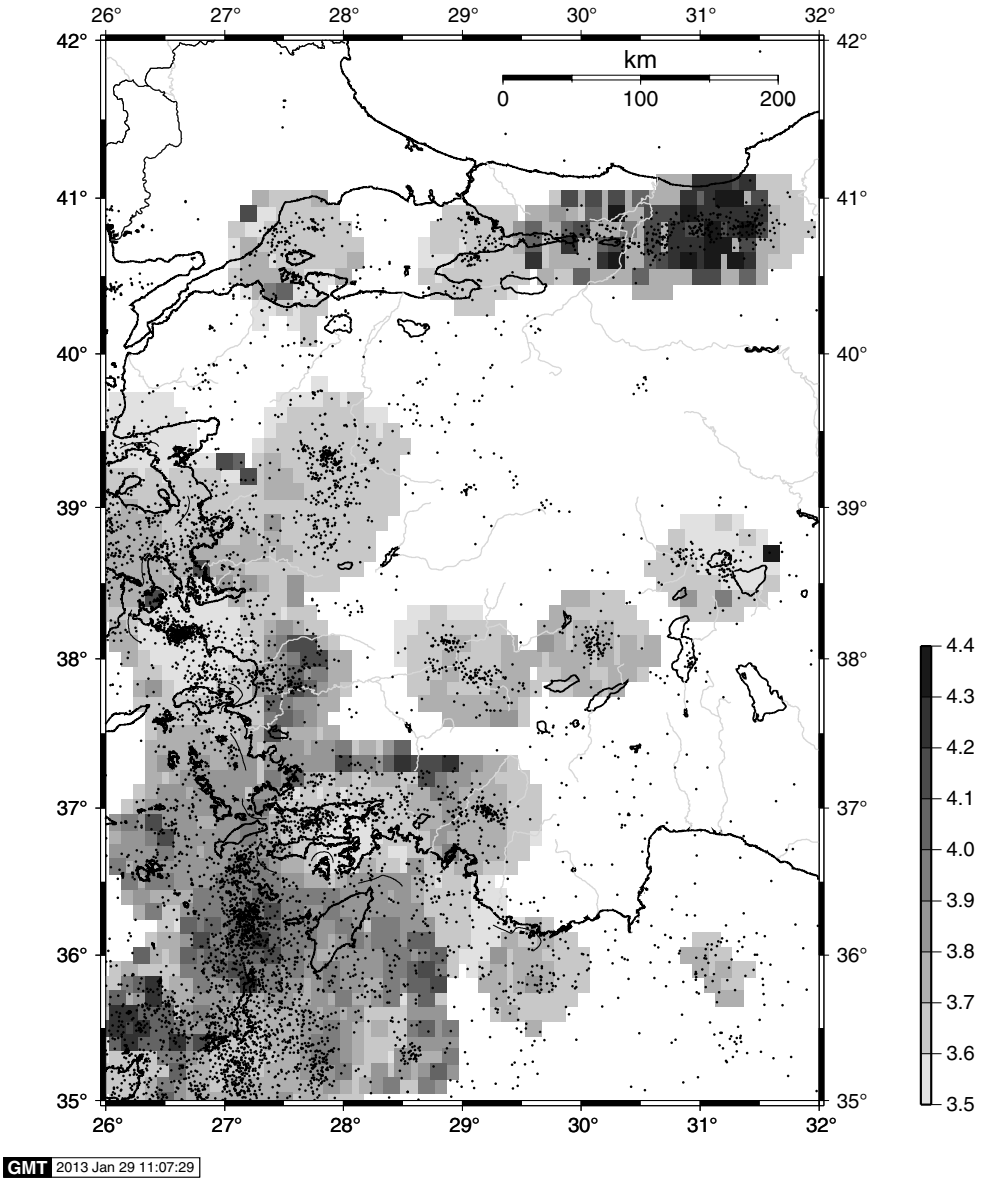

Figure 9. Map of M_c after 1995 in the study site, calculated in a grid $0.1° \times 0.1°$ by evaluating the goodness of fit in circular areas centered in the bins' centers and with 40 km radii. Calculations were only performed when the selected areas comprising at least 50 events and the magnitude range was more than 1.5 units. Seismicity since 1995 is also shown as dots.

size and higher M_c thresholds. The FMD was simulated by a G-R power law (as a function of minimum magnitude) until the maximum magnitude that the dataset includes and the parameters of the power law were evaluated using the maximum-likelihood estimate. In addition to this approach, synthetic catalogs were constructed following the defined G-R law, and then the number of events for each magnitude bin of the synthetic catalogs was compared with the corresponding observed one and with the respective number derived from the theoretical distribution. In this way, our method provided a discrete point of minimum residual value that can be considered as the completeness magnitude for a certain period.

The results were compared with those derived from the application of MAXC and the original GFT methods for the consistency of the three approaches to be tested. In general, there is a good agreement among them, especially when the catalog of a study period contains sufficient number of data, whereas there is a significant deviation among them for earlier periods exhibiting limited data. In these cases, the technique introduced here provides a more conservative selection of M_c, about 0.1–0.4 units higher than MAXC and GFT (90%). GFT(95%), on the contrary, demonstrates inordinately higher M_c values for some cases in comparison with all the other methods. There are also some datasets in which the 95% level cannot be achieved due to the relatively low sample size or the irregularities arising from the magnitude conversion procedure. The MGFT method is free from such behavior and therefore is more reliable when applied in datasets that demonstrate higher completeness level or for short time intervals containing limited number of events.

Our technique is demonstrated to be more stable than the original GFT and independent of the R-value selection, as well as being more conservative than the MAXC, which has already been shown to tend toward underestimating M_c. We are confident that the technique introduced here can be easily applied to other regions with relatively low detection level but with high seismic hazard, such as eastern Anatolia, the Aegean Sea, and the surrounding lands, the ultimate goal being reliable and feasibly achievable results.

Data and Resources

The earthquake catalog from the International Seismological Center, used in this paper, can be searched at http://www.isc.ac.uk/iscbulletin/search/bulletin/ (last accessed October 2012). Data were also obtained from the Kandilli Observatory and Earthquake Research Institute, Bogazici University, Istanbul, Turkey (http://www.koeri.boun.edu.tr/sismo/indexeng.htm; last accessed September 2012), the Geophysics Department of the Aristotle University of Thessaloniki (http://geophysics.geo.auth.gr/ss/station_index.html; last accessed December 2012), and the Institute of Geodynamics of the National Observatory of Athens (http://www.gein.noa.gr/en/; last accessed December 2012). The Generic Mapping Tools system, version 4.5.3 (www.soest.hawaii.edu/gmt, Wessel and Smith, 1998; last accessed May 2012) was used to plot some of the figures.

Acknowledgments

This work was partially supported by the research project titled as "Seismotectonic properties of the eastern Aegean: Implications on the stress field evolution and seismic hazard assessment in a tectonically complex area," GSRT 10 TUR/ 1–3–9, Joint Research and Technology Programmes 2010–2011, financed by the Ministry of Education of Greece. Geophysics Department, Aristotle University of Thessaloniki, Contribution Number 800/2013.

References

Aki, K. (1965). Maximum likelihood estimate of b in the formula $\log N = a - bM$ and its confidence limits, *Bull. Earthq. Res. Inst. Tokyo Univ.* **43,** 237–239.

Akkar, S., Z. Çağnan, E. Yenier, Ö. Erdoğan, M. A. Sandikkaya, and P. Gülkan (2010). The recently compiled Turkish strong motion database: Preliminary investigation for seismological parameters, *J. Seismol.* **14,** 457–479.

Ambraseys, N. N. (2000). Reappraisal of north-Indian earthquakes at the turn of the 20th century, *Curr. Sci.* **79,** 1237–1250.

Ambraseys, N. N., and C. F. Finkel (1995). *The Seismicity of Turkey and Adjacent Areas: A Historical Review, 1500–1800*, Muhittin Salih EREN, Istanbul, Turkey.

Ambraseys, N. N., and J. A. Jackson (1998). Faulting associated with historical and recent earthquakes in the Eastern Mediterranean region, *Geophys. J. Int.* **133,** 390–406.

Amorèse, D. (2007). Applying a change-point detection method on frequency–magnitude distributions, *Bull. Seismol. Soc. Am.* **97,** doi: 10.1785/0120060181.

Baba, A. B., E. E. Papadimitiou, B. C. Papazachos, C. A. Papaioannou, and B. G. Karakostas (2000). Unified local magnitude scale for earthquakes of south Balkan area, *Pure Appl. Geophys.* **157,** 765–783.

Bormann, P., and J. Saul (2008). The new IASPEI standard broadband magnitude m_B, *Seismol. Res. Lett.* **79,** 698–705.

Burton, P. W., Y. Xu, C. Qin, G. Tselentis, and E. Sokos (2004). A catalogue of seismicity in Greece and the adjacent areas for the twentieth century, *Tectonophysics* **390,** 117–127.

Cao, A. M., and S. S. Gao (2002). Temporal variation of seismic b-values beneath northeastern Japan island arc, *Geophys. Res. Lett.* **29,** doi: 10.1029/2001GL013775.

Castellaro, S., and P. Bormann (2007). Performance of different regression procedures on the magnitude conversion problem, *Bull. Seismol. Soc. Am.* **97,** 1167–1175.

Castellaro, S., F. Mulargia, and Y. Y. Kagan (2006). Regression problems for magnitudes, *Geophys. J. Int.* **165,** 913–930.

Deniz, A., and M. S. Yücemen (2010). Magnitude conversion problem for the Turkish earthquake data, *Nat. Hazards* **55,** 333–352.

Ekström, G., and A. M. Dziewonski (1988). Evidence of bias in estimation of earthquake size, *Nature* **332,** 319–323.

Ergin, K., U. Güçlü, and G. Aksay (1971). A catalog of earthquakes of Turkey and surrounding area (1965–1970), *Publ. Techn. Univ. Istanbul, Turkey* **28,** 184 pp.

Ergin, K., U. Güçlü, and Z. Uz (1967). A catalog of earthquakes for Turkey and surrounding area (11 A.D. to 1964 A.D.), *Publ. Techn. Univ. Istanbul, Turkey* **24,** 169 pp.

Fuller, W. A. (1987). *Measurement Error Models*, Wiley, New York, 440 pp.

Grünthal, G., R. Wahlström, and D. Stromeyer (2009). The unified catalog of earthquakes in central, northern, and northwestern Europe (CENEC)—updated and expanded to the last millennium, *J. Seismol.* **13,** doi: 10.1007/s10950-008-9144-9.

Güçlü, U., G. Altibans, and H. Eyidoğan (1986). A catalog of earthquakes of Turkey and surrounding area (1971–1975), *Publ. Techn. Univ. Istanbul, Turkey* **30,** 191 pp.

Habermann, R. E. (1987). Man-made changes of seismicity rates, *Bull. Seismol. Soc. Am.* **77,** 141–159.

Husen, S., and J. L. Hardebeck (2011). Understanding seismicity catalogs and their problems, *Community Online Resource for Statistical Seismicity Analysis* doi: 10.5078/corssa-55815573.

Hutton, K., J. Woessner, and E. Hauksson (2010). Earthquake monitoring in southern California for seventy-seven years (1932–2008), *Bull. Seismol. Soc. Am.* **100,** 423–446.

Johnston, A. C. (1996). Seismic moment assessment of earthquakes in stable continental regions—I. Instrumental seismology, *Bull. Seismol. Soc. Am.* **124,** 381–414.

Lolli, B., and P. Gasperini (2012). A comparison among general orthogonal regression methods applied to earthquake magnitude conversions, *Geophys. J. Int.* **190,** 1135–1151.

Mignan, A., and J. Woessner (2012). Estimating the magnitude of completeness for earthquake catalogs, *Community Online Resource for Statistical Seismicity Analysis* doi: 10.5078/corssa-00180805.

Mignan, A., M. J. Werner, S. Wiemer, C.-C. Chen, and Y.-M. Wu (2011). Bayesian estimation of the spatially varying completeness magnitude of earthquake catalogs, *Bull. Seismol. Soc. Am.* **101,** doi: 10.1785/0120100223.

Ogata, Y., and K. Katsura (1993). Analysis of the temporal and spatial heterogeneity of magnitude frequency distribution inferred from earthquake catalogs, *Geophys. J. Int.* **113,** 727–738.

Papazachos, B. C., and P. E. Comninakis (1969). Geophysical features of the Greek Island Arc and Eastern Mediterranean Ridge, *Com. Ren. Séances Conf. Reunie Madrid* **16,** 74–75.

Papazachos, B. C., V. G. Karakostas, A. A. Kiratzi, B. N. Margaris, C. B. Papazachos, and E. M. Scordilis (2002). Uncertainties in the estimation of earthquake magnitudes in Greece, *J. Seismol.* **6,** 557–570.

Papazachos, B. C., A. A. Kiratzi, and B. G. Karakostas (1997). Toward a homogeneous moment-magnitude determination for earthquakes in Greece and surrounding area, *Bull. Seismol. Soc. Am.* **87,** 474–483.

Pavlis, G. L. (1986). Appraising earthquake hypocenter location errors – a complete, practical approach for single-event locations, *Bull. Seismol. Soc. Am.* **76,** 1699–1717.

Pinar, N., and E. Lahn (1952). Turkish earthquake catalog with descriptions, *Publ. Techn. Univ. Istanbul, Turkey* **36,** 153 pp.

Rydelek, P. A., and I. S. Sacks (1989). Testing the completeness of earthquake catalogs and the hypothesis of self-similarity, *Nature* **337,** 251–253.

Schorlemmer, D., and J. Woessner (2008). Probability of detecting an earthquake, *Bull. Seismol. Soc. Am.* **98,** doi: 10.1785/0120070105.

Scordilis, E. M. (2006). Empirical global relations converting M_s and m_b to moment magnitude, *J. Seismol.* **10,** 225–236.

Soysal, H., S. Sipahioğlu, D. Kolçak, and Y. Altinok (1981). Historical earthquake catalogue of Turkey and surrounding area (2100 B.C.–1900 A.D.), *Publ. Techn. Univ. Istanbul, Turkey*, Number TBAG-341.

Tan, O., M. G. Tapirdamaz, and A. Yörük (2008). The earthquake catalogues for Turkey, Turkish, *J. Earth Sci.* **17,** 405–418.

Taylor, D. W. A., J. A. Snoke, I. S. Sacks, and T. Takanami (1990). Non-linear frequency-magnitude relationship for the Hokkaido corner, Japan, *Bull. Seismol. Soc. Am.* **80,** 605–609.

Ulusay, R., E. Tuncay, H. Sonmez, and C. Cokceoglu (2004). An attenuation relationship based on Turkish strong motion data and iso-accelaration map of Turkey, *Eng. Geol.* **74,** 265–291.

Wason, H. R., R. Das, and M. L. Sharma (2012). Magnitude conversion problem using general orthogonal regression, *Geophys. J. Int.* **190,** 1091–1096.

Wessel, P., and W. H. F. Smith (1998). New, improved version of the Generic Mapping Tools released, *Eos Trans. AGU* **79,** 579.

Wiemer, S., and M. Wyss (2000). Minimum magnitude of completeness in earthquake catalogs: Examples from Alaska, the Western United States, and Japan, *Bull. Seismol. Soc. Am.* **90,** no. 4, 859–869.

Woessner, J., and S. Wiemer (2005). Assessing the quality of earthquake catalogs: Estimating the magnitude of completeness and its uncertainty, *Bull. Seismol. Soc. Am.* **95,** 684–698.

Yadav, R. B. S., P. Bormann, B. K. Rastogi, M. C. Das, and S. Chopra (2009). A homogeneous and complete earthquake catalog for northeast India and the adjoining region, *Seismol. Res. Lett.* **80,** doi: 10.1785/gssrl.80.4.609.

Zechar, J. D. (2010). Evaluating earthquake predictions and earthquake forecasts: A guide for students and new researchers, *Community Online Resource for Statistical Seismicity Analysis*, doi: 10.5078/corssa-77337879.

Appendix

We derived relations between M_w and other magnitude scales published by different institutions, and then we applied the most reliable of them after taking into consideration the sample size, the rms error, the linear correlation coefficient (R^2), and the uncertainties of the linear regression parameters a and b. To obtain these relations we avoided using the ordinary least-squares method, which assumes that there are no uncertainties in the values of the independent variable. This may introduce systematic errors in magnitude conversion, apparent catalog incompleteness, and significant bias in the estimates of the b-value (Castellaro *et al.*, 2006). Alternatively, we applied the general orthogonal regression technique in order to avoid such artifacts (Castellaro and Gormann, 2007; Deniz and Yucemen, 2010; Lolli and Gasperini, 2012; Wason *et al.*, 2012). According to this method, the projection of the independent variable is done along a weighted orthogonal distance from the linear fitting curve. The values of the slope b and intercept a are estimated by Fuller (1987) formulas as

$$b = \frac{S_y^2 - nS_x^2 + \sqrt{(S_y^2 - nS_x^2)^2 + 4nS_{xy}^2}}{2S_{xy}} \tag{A1}$$

$$a = \langle y \rangle - b\langle x \rangle, \tag{A2}$$

in which S_x and S_y are the standard deviations of x and y variables, respectively, S_{xy} is the sample covariance between x and y, $\langle y \rangle$ and $\langle x \rangle$ are the average values of y and x, and $n = [\sigma_{(y)}/\sigma_{(x)}]^2$ is the error variance ratio. Because the standard errors of the available data are unknown, we set $n = 1$. Castellaro *et al.* (2006) showed that even if the applied values of the ratios of the errors are different from the real one, the orthogonal regression method still performs better than the ordinary least squares. The errors of the slope and the intercept given the sample size N are expressed as follows:

$$\hat{\sigma}_\beta^2 = \frac{(\hat{\sigma}_x + \hat{\sigma}_u)S_u - (-b\hat{\sigma}_u)^2}{(N-1)\hat{\sigma}_x^2} \tag{A3}$$

and

$$\hat{\sigma}_a^2 = \frac{S_u}{N} + \langle x \rangle^2 \hat{\sigma}_\beta^2, \tag{A4}$$

in which

$$\hat{\sigma}_x = \frac{\sqrt{(S_y^2 - nS_x^2)^2 + 4nS_{xy}^2} - (S_y^2 - nS_x^2)}{2n}, \tag{A5}$$

$$\hat{\sigma}_u = \frac{(S_y^2 + nS_x^2) - \sqrt{(S_y^2 - nS_x^2)^2 + 4nS_{xy}^2}}{2n}, \tag{A6}$$

and

$$S_u = \frac{(N-1)(n-b^2)\hat{\sigma}_u}{N-2}. \tag{A7}$$

School of Geology, Geophysics Department
Aristotle University of Thessaloniki
GR54124 Thessaloniki, Greece
kleptoka@geo.auth.gr
vkarak@geo.auth.gr
ritsa@geo.auth.gr
adaggela@yahoo.gr
(K.M.L., V.G.K., E.E.P., A.K.A.)

TUBITAK Marmara Research Center
Earth and Marine Sciences Institute
Gebze TR–41470 Kocaeli, Turkey
Tan@mam.gov.tr
(O.T.)

EXPEC Advance Research Center Saudi Arabian Oil Company (ARAMCO)
P.O. BOX 5074
Dhahran, 31311
Saudi Arabia
sedatinan64@gmail.com
(S.I.)

Manuscript received 17 May 2012